PHYSICAL REVIEW B **78**, 174509 (2008)

Alternating dynamic state self-generated by internal resonance in stacks of intrinsic Josephson junctions

A. E. Koshelev
Materials Science Division, Argonne National Laboratory, Argonne, Illinois 60439, USA
(Received 1 April 2008; revised manuscript received 10 October 2008; published 7 November 2008)

Intrinsic Josephson-junction stacks realized in high-temperature superconductors provide a very attractive base for developing coherent sources of electromagnetic radiation in the terahertz frequency range. A promising way to synchronize phase oscillations in all the junctions is to excite an internal cavity resonance. We demonstrate that this resonance promotes the formation of an alternating coherent state, in which the system spontaneously splits into two subsystems with different phase-oscillation patterns. There is a static phase shift between the oscillations in the two subsystems, which changes from 0 to 2π in a narrow region near the stack center. The oscillating electric and magnetic fields are almost homogeneous in all the junctions. The formation of this state promotes efficient pumping of the energy into the cavity resonance leading to strong resonance features in the current-voltage dependence.

DOI: 10.1103/PhysRevB.78.174509 PACS number(s): 74.50.+r, 74.81.Fa, 85.25.Cp, 74.72.Hs

I. INTRODUCTION

High-temperature layered superconductors, such as $Bi_2Sr_2CaCu_2O_8$ (BSCCO), are composed of two-dimensional superconducting CuO_2 layers coupled via the Josephson effect.[1] The large packing density of the intrinsic junctions makes these compounds very attractive for developing coherent generators of electromagnetic radiation based on the ac Josephson effect. Moreover, a large value of the superconducting gap allows to bring the operation frequency of potential devices into the practically important terahertz range. To develop a powerful source, the major challenge is to synchronize the oscillations of the superconducting phases in a large number of junctions. One possible way to synchronization is to use interactions between the junctions due to generated external radiation.[2] In this case, for efficient coupling to the radiation field, a junction stack (mesa) must have small lateral size (<10 μm) and contain a very large number of junctions ($>10^4$). Such mesa would be a frequency-tunable source with the maximum power conversion efficiency up to 30%. The obvious technological challenge of this design is a requirement to fabricate mesa with such large number of almost identical junctions.

A very promising different route to efficient synchronization is to excite an internal cavity resonance in finite-size mesas,[3,4] which can entrain oscillations in a very large number of junctions. The frequency of this so-called in-phase Fiske mode is set by the lateral size of the mesa, which has to be rather wide (40–100 μm). The experimental demonstration of this mechanism[3] has brought the quest for superconducting terahertz sources to a new level.

In general, a mechanism of pumping energy into the cavity mode is a nontrivial issue. Homogeneous phase oscillations at zero magnetic field do not couple to the Fiske modes. Such coupling can be facilitated by introducing an external modulation of the Josephson critical current density.[4] In this case the amplitudes of the generated standing wave and of the produced radiation are proportional to the strength of modulation.

In this paper we explore an interesting alternative possibility. Numerically solving the dynamic equations for the Josephson-junction stacks, we found that near the resonance an inhomogeneous synchronized state is formed. In this state, the system spontaneously splits into two subsystems with different phase-oscillation patterns formally corresponding to fluxon-antifluxon oscillations.

Inspired by numerics, we also succeeded to build such solution analytically. The phase oscillations in two subsystems have a static phase shift which has a soliton-shape coordinate dependence, changing from 0 at one side to 2π at other side (phase kink). This change occurs within the narrow region near the center of the stack and the width of this region shrinks when approaching to the resonance. In spite of the difference in the phase-oscillation patterns for the two subsystems, the oscillating electric and magnetic fields are almost identical in all the junctions. Independently, such state was also reported by Lin and Hu.[5] The formation of this state strongly enhances coupling to the resonance mode and promotes efficient pumping of energy into the cavity resonance.

II. DYNAMIC EQUATIONS

The dynamic equations for the Josephson-junction stacks have been derived in Ref. 6 and have been used in numerous theoretical studies.[7] We present these equations in the form of coupled time-evolution equations for reduced electric and magnetic fields e_n and h_n, phase differences φ_n, and the in-plane phase gradients k_n,

$$\frac{\partial e_n}{\partial \tau} = -\nu_c e_n - g(u)\sin\theta_n + \frac{\partial h_n}{\partial u} + \tilde{j}_z(u,n,\tau), \tag{1a}$$

$$\frac{\partial \theta_n}{\partial \tau} = e_n, \tag{1b}$$

$$\nu_{ab}\frac{\partial k_n}{\partial \tau} = -[k_n + h_n - h_{n-1}] + \tilde{j}_{ab}(u,n,\tau), \tag{1c}$$

$$h_n = \ell^2\left(\frac{\partial \theta_n}{\partial u} - k_{n+1} + k_n\right). \tag{1d}$$

TABLE I. Units of physical variables. Here ω_p is plasma frequency, λ_J is the Josephson length, s is the interlayer period, λ is the in-plane London penetration depth, γ is the anisotropy factor, and j_J is the Josephson current density.

Variable	Time τ	Coordinate u	Phase gradient k_n	Electric field e_n	Magnetic field h_n	Current density j
Unit	$1/\omega_p$	λ_J	$1/\lambda_J$	$\Phi_0\omega_p/2\pi cs$	$\Phi_0/2\pi\gamma\lambda^2$	j_J

The units and definitions of parameters are summarized in Table I and its caption. These reduced equations depend on three parameters: $\nu_c=4\pi\sigma_c/\varepsilon_c\omega_p$, $\nu_{ab}=4\pi\sigma_{ab}/\varepsilon_c\omega_p\gamma^2$, and $\ell=\lambda/s$, where σ_c and σ_{ab} are components of the quasiparticle conductivity. We also include possible noise currents $\tilde{j}_z(u,n,t)$ and $\tilde{j}_{ab}(u,n,t)$, which are defined by the correlation functions as

$$\langle \tilde{j}_z(0,0,0)\tilde{j}_z(u,n,\tau)\rangle = 2\nu_c\tilde{T}\delta(u)\delta_n\delta(\tau),$$

$$\langle \tilde{j}_{ab}(0,0,0)\tilde{j}_{ab}(u,n,\tau)\rangle = 2\nu_{ab}\tilde{T}\delta(u)\delta_n\delta(\tau).$$

The noise amplitude is determined by the effective temperature $\tilde{T}$. We neglected the in-plane displacement current, which would give a term $\sim\partial^2 k_n/\partial\tau^2$, because relevant frequencies are much smaller than the in-plane plasma frequency. The time-evolution presentation of the dynamic equations (1a)–(1d) allows for straightforward numerical implementation, which is discussed in the Appendix.

We simulated a stack containing N junctions ($1\le n\le N$), having a width of $L\lambda_J$ ($0<u<L$), and assuming that the dynamic state is homogeneous in the third direction. We study the voltage range corresponding to the Josephson frequencies close to the lowest in-phase resonance frequency $\omega_1=\pi\ell/L$. The function $g(u)=1-2r(u-L/2)/L$ in Eq. (1a) describes a linear modulation of the Josephson current density, which provides coupling to this mode for c-axis homogeneous oscillations.[4] Realistic simulations have to take into account boundary conditions accounting for radiation.[4] However, for short mesas, $N\lesssim 100$, the radiation influences weakly the structure of internal dynamic states. As our purpose is to probe the qualitative structure of these states, we use simple nonradiative boundary conditions at the edges: $k_n=0$ and $\partial\varphi_n/\partial u=\mp I/2\ell^2$ for $u=0,L$, where I is the transport current flowing through the stack. We also assume metallic contacts at the top and the bottom: $k_0=k_{N+1}=0$.

III. NUMERICAL RESULTS

Figure 1 shows the current-voltage dependences (CVDs) obtained for representative system parameters listed in the plot and for two values of the modulation parameter $r=0$ and 0.4. These dependences have been obtained with increasing current and without noise. We observe a strong resonance enhancement of the current due to the excitation of the internal cavity resonance. Without noise, the emerging state is sensitive to the initial configuration. If we start with a c-axis homogeneous state, it remains homogeneous up to certain current. In this case the resonance is excited due to the finite modulation and it is well described by theory developed in Ref. 4. However, if we add a small n-dependent perturbation to the phase at the start of every current run, the homogeneous state blows up and the system organizes itself into a coherent inhomogeneous state. We also studied a system without modulation using an inhomogeneous state as initial state and found that the corresponding CVD is practically undistinguishable from the one for the modulated system. Therefore, the modulation of the critical current density triggers the transition to the inhomogeneous state; but once being formed, this state is not sensitive to the modulation any more.

To understand the nature of the inhomogeneous state, we show in Fig. 2 the time evolution of the phase and electric field for the eight bottom junctions for $j=0.18$. We see that the system splits into two alternating subsystems with different phase dynamics, corresponding to fluxon-antifluxon oscillations. In the first half period vortices nucleate at the left side in even junctions, rapidly move to the center, then, after slow motion near the center, rapidly annihilate at the right side. Immediately after that, in the second half period, antivortices nucleate at the right side in the odd junctions, move to the left in a similar way, and annihilate at the left side. Inspite of the difference in the phase dynamics between the two subsystems, the electric and magnetic fields are almost identical in all junctions. For the electric field, this can be seen from the lower plots of Fig. 2. The dominating contri-

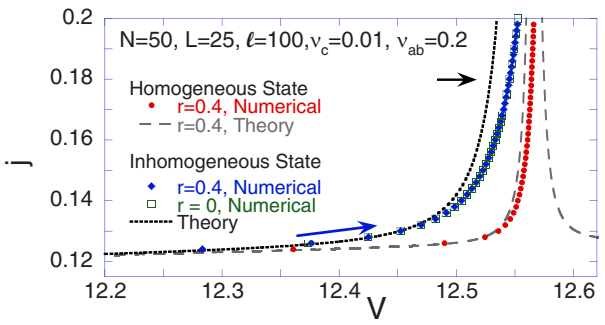

FIG. 1. (Color online) Simulated and theoretical CVDs in the vicinity of the resonance voltage for different states with $V=\langle e_n\rangle=\omega$. Small circles show the dependence obtained for $r=0.4$ and c-axis homogeneous initial state, which remains homogeneous with increasing current. The theoretical CVD for this state (Ref. 4) is shown by gray dashed line. Small filled diamonds show the CVD for $r=0.4$ and inhomogeneous state, which was self-generated when small n-dependent perturbation was added to the phase in the beginning run for each current value. The open squares represents the CVD for $r=0$ when the inhomogeneous state has been used as the initial state at starting current. The inhomogeneous state is not sensitive to modulation. Dotted black line shows the theoretical curve for the inhomogeneous state based on Eqs. (6) and (13).

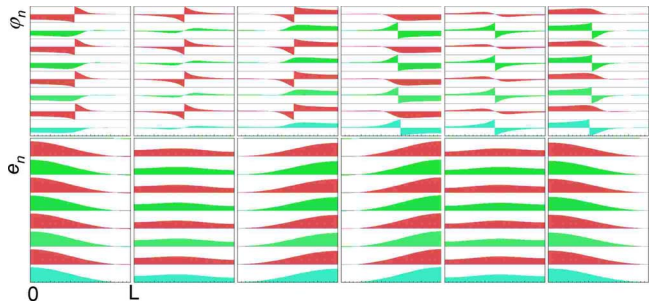

FIG. 2. (Color online) Snapshots of the phase and electric-field configurations in the eight bottom junctions for the same parameters as in Fig. 1 and $j=0.18$ marked by the arrow (see also animations in Ref. 8). The phases are reduced to the interval $[-\pi,\pi]$, so that jumps formally correspond to centers of the Josephson vortices. The dynamic state corresponds to alternating nucleation, motion, and annihilation of vortices in the even junctions and antivortices in the odd junctions. Vortex velocities near the edges much larger than near the center. In between third and 4th configurations, jumplike annihilation of fluxons and nucleation of antifluxons take place at the right side. The lower plots show that the electric field is homogeneous in all junctions and has space-time dependence corresponding to the fundamental mode. The annihilation and nucleation events correspond to maxima of electric fields at the edges.

bution to the oscillating electric field is given by the fundamental cavity mode $e_n \propto \cos(\pi u/L)$.

The homogeneity of the electric field implies that there is a static phase shift between the phase oscillations in the two subsystems. Figure 3 shows the cosine of half of this phase shift at different currents. One can see that the phase shift has the shape of a soliton and its width shrinks with increasing current.

A. Influence of noise

We studied stability of the alternating state with respect to the thermal noise. Figure 4 shows the current-voltage dependences for different values of the effective temperature. All

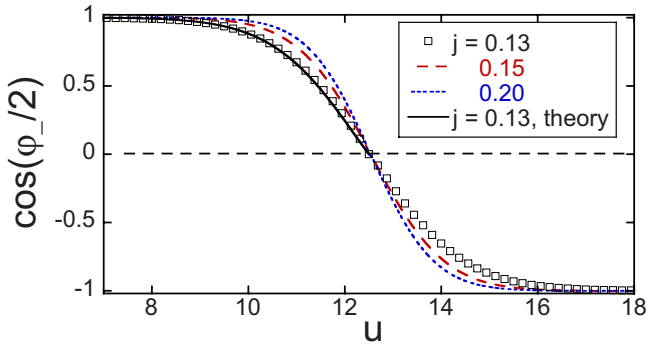

FIG. 3. (Color online) Cosine of half static phase shift between phases in two subsystems at different currents. One can see that the phase shift has shape of soliton (kink) and it narrows with approaching to the resonance. The solid line shows theoretical curve based on Eq. (12) and using Eqs. (9), (10), and (13) for $j=0.13$. This function determines the coupling of the homogeneous Josephson oscillations to the internal resonance mode.

other parameters are the same as in Fig. 1 and the Josephson coupling is homogeneous, $r=0$. We found that in the presence of noise the system spontaneously transfers into the alternating state, indicating stability of this state. With increasing noise, the resonance current enhancement at a given voltage is suppressed and maximum achievable current also decreases. Nevertheless, the coherent state survives up to a rather high level of noise.

Note that the noise in our two-dimensional model is not fully realistic. In real mesas, the thermal noise immediately induces dependence of the variables on the third coordinate and this makes the system three dimensional. The influence of noise is presented here only for as a check for stability and for qualitative illustration. The temperature has to be considered as effective parameter controlling the strength of noise.

IV. ANALYTICAL SOLUTION

To study the dynamic state analytically, we assume that the system is split into two alternating subsystems: $\varphi_{2m+1}=\varphi_1$ and $\varphi_{2m}=\varphi_2$.[9] Introducing new variables $\varphi_+=(\varphi_1+\varphi_2)/2$ and $\varphi_-=\varphi_2-\varphi_1$ and excluding other variables, we derive from Eq. (1) for $\ell \gg 1$

$$\frac{\partial^2\varphi_+}{\partial\tau^2}+\nu_c\frac{\partial\varphi_+}{\partial\tau}-\ell^2\frac{\partial^2\varphi_+}{\partial u^2}=-\sin\varphi_+\cos(\varphi_-/2), \tag{2a}$$

$$\frac{\partial^2\varphi_-}{\partial\tau^2}+\nu_c\frac{\partial\varphi_-}{\partial\tau}-\frac{1}{4}\left(1+\nu_{ab}\frac{\partial}{\partial\tau}\right)\frac{\partial^2\varphi_-}{\partial u^2}=-2\sin(\varphi_-/2)\cos\varphi_+. \tag{2b}$$

We now obtain a self-consistent approximate solution of these equations for the dynamic state when the Josephson frequency $\omega=\langle e_n\rangle$ is close to the resonance frequency $\omega_1=\pi\ell/L$. We will show that φ_- is almost static. In this case the equation for φ_+ coincides with the phase equation for the Josephson junction with modulated Josephson current density[4] with modulation function $g(u)=\cos(\varphi_-/2)$ (see Fig. 3). Near the resonance frequency, we make the mode projection for φ_+,

$$\varphi_+(u,\tau)\approx\omega\tau+\mathrm{Re}[\psi\exp(-i\omega\tau)]\cos(\pi u/L), \tag{3}$$

and, assuming $|\psi|\ll 1$, we obtain

$$\psi\approx\frac{ig_-}{\omega^2-\omega_1^2+i\nu_c\omega} \tag{4}$$

with

$$g_-=\frac{2}{L}\int_0^L\cos(\pi u/L)\cos(\varphi_-/2)du \tag{5}$$

being the coupling parameter. This solution determines the CVD, which takes into account resonance enhancement of the Josephson current $\delta j\approx\langle\cos(\varphi_-/2)\sin\varphi_+\rangle$ (Ref. 4) as

$$j(V)\approx\nu_cV+\frac{g_-^2\nu_cV/4}{(\omega_1^2-V^2)^2+(\nu_cV)^2}. \tag{6}$$

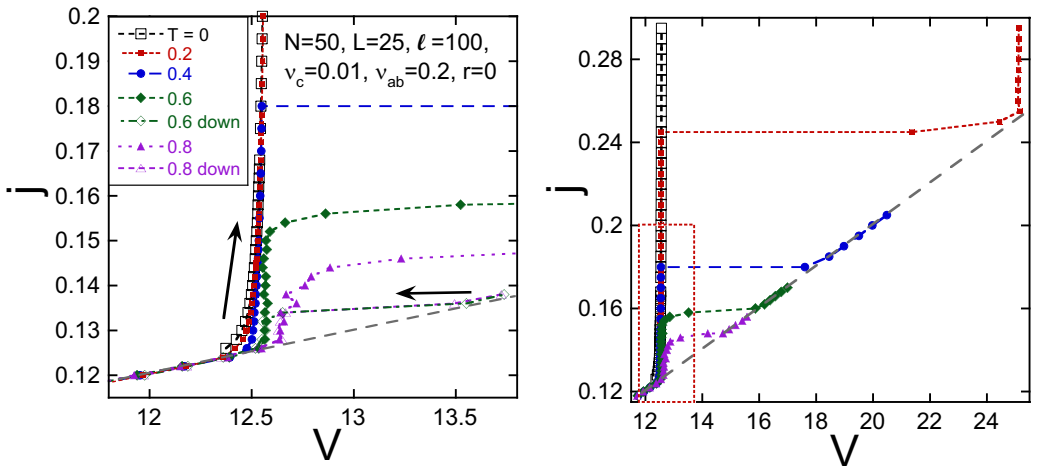

FIG. 4. (Color online) Influence of thermal noise on the current-voltage dependences. The left plot shows behavior near the resonance while the right plot shows the current-voltage dependences in the extended range (the dotted rectangle marks the region shown in the left plot). Most dependences are obtained with increasing the current. The left plot also shows decreasing current scans for $\tilde{T}=0.6$ and 0.8. The coherent state survives up to certain value of current, which is suppressed by noise. At this current the system typically jumps into incoherent state. For $\tilde{T}=0.2$ the system jumps to the higher-resonance state.

To evaluate $\varphi_-(u,\tau)$, we split it into static and dynamic parts: $\varphi_-(u,\tau)=\bar{\varphi}_-(u)+\tilde{\varphi}_-(u,\tau)$. Further analysis shows that $\tilde{\varphi}_-(u,\tau)\ll 1$. The static part is determined by

$$d^2\varphi_-/du^2 - 8C_+(u)\sin(\varphi_-/2)=0 \tag{7}$$

with $C_+(u)\equiv\langle\cos\varphi_+\rangle$. Using Eqs. (3) and (4), we obtain

$$C_+(u)\approx C_1\cos(\pi u/L) \tag{8}$$

with

$$C_1=-\frac{\mathrm{Im}[\psi]}{2}=-\frac{g_-}{2}\frac{\omega^2-\omega_1^2}{(\omega^2-\omega_1^2)^2+(\nu_c\omega)^2}. \tag{9}$$

Consider the region near the midpoint $u=L/2$, where the static cosine can be approximated by the linear function $C_+(u)\approx C_1(\pi/L)(L/2-u)$. Using the substitution

$$v=(u-L/2)/l_s,\quad l_s=(L/8\pi C_1)^{1/3}, \tag{10}$$

we can reduce Eq. (7) near the midpoint to the dimensionless form

$$d^2\varphi_-/dv^2+v\,\sin(\varphi_-/2)=0. \tag{11}$$

This equation allows for the soliton solution in which φ_- changes from 0 to 2π within $|v|\sim 1$, corresponding to $|u-L/2|\sim l_s$, and has the symmetry $\varphi_-(v)=2\pi-\varphi_-(-v)$. Typically, $l_s\ll L$ meaning that the linear expansion for $C_+(u)$ is valid in the soliton core and Eq. (11) accurately determines its shape. Numerically solving Eq. (11), we interpolate the solution as

$$\varphi_-(v)\approx\pi\exp\{-(\sqrt{2}/3)[(|v|+C_v)^{3/2}-C_v^{3/2}]\} \tag{12}$$

for $v<0$ with $C_v\approx 0.5129$.

To evaluate the coupling constant (5), we note that $\cos(\varphi_-/2)$ changes from 1 to -1 within a narrow region near the midpoint $|u-L/2|\sim l_s$ meaning that, up to terms $\sim(l_s/L)^2$, $\cos(\varphi_-/2)$ can be approximated by $\mathrm{sgn}(L/2-u)$ which gives $g_-\approx 4/\pi$. Surprisingly, this self-generated step-like modulation provides the maximum possible coupling to the resonance mode. Correction to g_- of the order of $(l_s/L)^2$ due to the finite soliton width can be evaluated as

$$\delta g_-=\frac{4}{L}\int_0^{L/2}\cos\left(\frac{\pi u}{L}\right)\left(\cos\frac{\varphi_-}{2}-1\right)du\approx -0.464\frac{4\pi l_s^2}{L^2}.$$

Adding this correction and using Eqs. (9) and (10), the total coupling parameter can be written as

$$g_-\approx\frac{4}{\pi}\left\{1-1.817\left[\frac{(\omega_1^2-\omega^2)L^2}{(\omega^2-\omega_1^2)^2+(\nu_c\omega)^2}\right]^{-2/3}\right\}. \tag{13}$$

As $g_-\sim 1$, the used linear approximation $|\psi|\ll 1$ is valid only at $|\omega^2-\omega_1^2|>1$.

To evaluate the time-dependent part of φ_-, we represent it in the complex form $\tilde{\varphi}_-(\tau,u)=\mathrm{Re}[\bar{\varphi}_-(u)\exp(-i\omega\tau)]$, and separating the time-dependent part of Eq. (2b), we derive the equation for the complex amplitude

$$(\omega^2+i\nu_c\omega)\bar{\varphi}_-+\frac{1-i\nu_{ab}\omega}{4}\frac{\partial^2\bar{\varphi}_-}{\partial u^2}=2\sin\frac{\bar{\varphi}_-}{2}.$$

For $\omega\gg 1$, we estimate $\bar{\varphi}_-\approx 2\sin(\bar{\varphi}_-/2)/\omega^2\ll 1$, which justifies usage of the static approximation for φ_-.

In Fig. 3 we present the theoretical result for $\cos(\varphi_-/2)$ at $j=0.13$ based on Eq. (12). It accurately describes the numerical data. The theoretical prediction for the CVD based on Eqs. (6) and (13) is shown in Fig. 1. The linear approximation describes well the numerical data for voltages not too close to the resonance. Due to the enhancement of nonlinearities in the vicinity of the resonance, the analytical result overestimates the current increase.

V. DISCUSSION

The found state looks similar to the fluxon-antifluxon oscillations in a single junction.[10] These oscillations appear as

a result of a parametric instability of the homogeneous oscillations[11] and lead to the so-called zero-field steps in the CVDs.[12] The Josephson frequency of such step is twice the frequency of the involved resonance. In spite of the apparent similarity, there are essential qualitative differences. In our case, the frequency coincides with the resonance frequency. The dynamic configurations are also very different. In the case of a single junction, a well-developed fluxon nucleates at one side, moves with Swihart velocity to the other side, and converts to the antifluxon there, which then moves back again with constant velocity.[10] In our case, there is a region statically located near the center where rapid phase change $\pm\pi$ is localized corresponding to 2π phase change in ϕ_-. As a consequence, the centers of fluxons and antifluxons, formally defined as points where the phases are commensurate with $\pm\pi$, spend most time near the center and very rapidly jump to and from the edges (see Fig. 2). Moreover, the fluxon interpretation of our oscillations is somewhat artificial, as there are no well-defined localized soliton excitations moving across the junctions.

The alternating state is a plausible candidate for the coherent state responsible for resonant terahertz emission reported in Ref. 3. Even though we did not use boundary conditions accounting for the radiation, it is clear that the generation of such state would lead to powerful emission. In fact, for short mesas the radiation influences weakly the structure of the internal states and therefore it cannot destroy the coherent state. The emission can be approximately computed from the oscillating electric fields at the edges.[4] The radiation may contribute to the resonance damping in the mode amplitude (4). This contribution can be taken into account by adding to ν_c the radiation-damping term.[4] The experimental resonance features in the CVDs are much weaker then the theoretical ones. The possible mechanisms reducing the amplitude of the resonance include noise, c-axis inhomogeneities, and additional damping channels not taken into account by the theoretical model.

ACKNOWLEDGMENTS

The author would like to thank U. Welp, L. Bulaevskii, K. Gray, M. Tachiki, and X. Hu for useful discussions. This work was supported by the US DOE, Office of Science under Contract No. DE-AC02–06CH11357.

APPENDIX: NUMERICAL PROCEDURE

We implement numerical solution of Eq. (1) as follows. Space and time discretization is performed using staggered grid. For coordinate, $\theta_n(u,\tau)$ and $e_n(u,\tau)$ are defined at the points $u=(j-1/2)d_u$, while $k_n(u,\tau)$ and $h_n(u,\tau)$ are defined at the points $u=jd_u$ (see Fig. 5). For time, e_n is defined at $\tau=md_\tau$ while θ_n, k_n, and h_n are defined at $\tau=(m+1/2)d_\tau$;

$$\theta_{n,j}^{m+1/2}=\theta_n[(j-1/2)d_u,(m+1/2)d_\tau],$$

$$e_{n,j}^{m}=e_n[(j-1/2)d_u,md_\tau],\quad 1<j<J,$$

$$k_{n,j}^{m+1/2}=k_n[(j-1)d_u,(m+1/2)d_\tau],$$

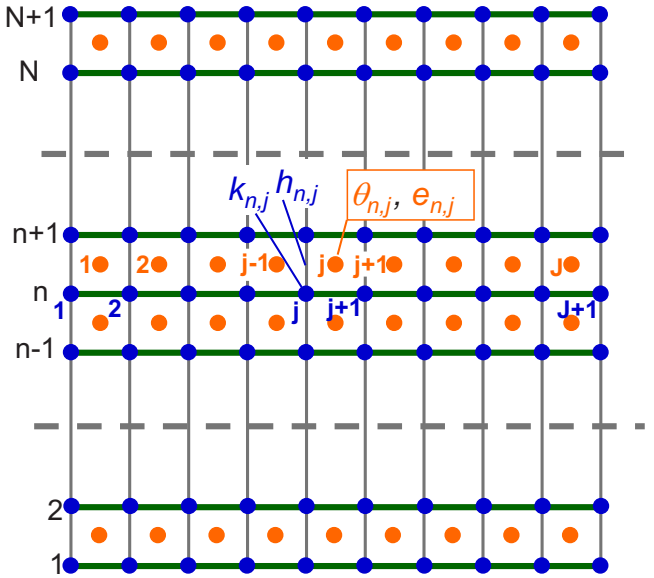

FIG. 5. (Color online) Illustration of the discretization scheme.

$$h_{n,j}^{m+1/2}=h_n[(j-1)d_u,(m+1/2)d_\tau],\quad 1<j<J+1.$$

We discretize equations as

$$\frac{e_{n,j}^{m+1}-e_{n,j}^{m}}{d_\tau}=-\nu_c\frac{e_{n,j}^{m+1}+e_{n,j}^{m}}{2}-g_j\sin\theta_{n,j}^{m+1/2}+\frac{h_{n,j+1}^{m+1/2}-h_{n,j}^{m+1/2}}{d_u}+\tilde{j}_{z,n,j}^{m+1/2},\tag{A1}$$

$$\frac{\theta_{n,j}^{m+3/2}-\theta_{n,j}^{m+1/2}}{d_\tau}=e_n^{m+1},\tag{A2}$$

$$\frac{k_{n,j}^{m+3/2}-k_{n,j}^{m+1/2}}{d_\tau}=-\frac{1}{\nu_{ab}}\left(\frac{k_{n,j}^{m+3/2}+k_{n,j}^{m+1/2}}{2}+\frac{h_{n,j}^{m+3/2}+h_{n,j}^{m+1/2}}{2}-\frac{h_{n-1,j}^{m+3/2}+h_{n-1,j}^{m+1/2}}{2}+\tilde{j}_{ab,n,j}^{m+1}\right),\tag{A3}$$

$$h_{n,j}^{m+3/2}=\ell^2\left(\frac{\theta_{n,j}^{m+3/2}-\theta_{n,j-1}^{m+3/2}}{d_u}-k_{n+1,j}^{m+3/2}+k_{n,j}^{m+3/2}\right),\tag{A4}$$

where $\tilde{j}_{z,n,j}^{m+1/2}$ and $\tilde{j}_{ab,n,j}^{m+1}$ are independent Gaussian variables with $\langle(\tilde{j}_{z,n,j}^{m+1/2})^2\rangle=2\nu_cT/d_ud_\tau$ and $\langle(\tilde{j}_{ab,n,j}^{m})^2\rangle=2\nu_{ab}T/d_ud_\tau$.

The first two equations allow for direct time advance of $e_{n,j}$ and $\theta_{n,j}$,

$$e_{n,j}^{m+1}=\left(\frac{1}{d_\tau}+\frac{\nu_c}{2}\right)^{-1}\left[\left(\frac{1}{d_\tau}-\frac{\nu_c}{2}\right)e_{n,j}^{m}-g_j\sin\theta_{n,j}^{m+1/2}+\frac{h_{n,j+1}^{m+1/2}-h_{n,j}^{m+1/2}}{d_u}+\tilde{j}_{z,n,j}^{m+1/2}\right],$$

$$\theta_{n,j}^{m+3/2}=\theta_{n,j}^{m+1/2}+d_\tau e_n^{m+1}.$$

Substitution of $h_{n,j}^{m+3/2}$ and $h_{n-1,j}^{m+3/2}$ from Eq. (A4) into Eq. (A3) leads to the tridiagonal linear system for $k_{n,j}^{m+3/2}$,

$$\ell^2 k_{n+1,j}^{m+3/2} - \left(1 + \frac{2\nu_{ab}}{d_\tau} + 2\ell^2\right) k_{n,j}^{m+3/2} + \ell^2 k_{n-1,j}^{m+3/2}$$
$$= \left(1 - \frac{2\nu_{ab}}{d_\tau}\right) k_{n,j}^{m+1/2}$$
$$+ \ell^2 \frac{\theta_{n,j}^{m+3/2} - \theta_{n,j-1}^{m+3/2} - \theta_{n-1,j}^{m+3/2} + \theta_{n-1,j-1}^{m+3/2}}{d_u}$$
$$+ h_{n,j}^{m+1/2} - h_{n-1,j}^{m+1/2} + 2\tilde{j}_{ab,n,j}^{m+1}$$

for $n=2,\ldots,N$ with $k_{1,j}^{m+3/2}=0$, $k_{N+1,j}^{m+3/2}=0$. Solving this system, we advance $k_{n,j}$. After finding $k_{n,j}^{m+3/2}$, we update $h_{n,j}^{m+3/2}$ using Eq. (A4).

This implicit numerical scheme is expected to be stable up to $d_\tau \lesssim d_u/\ell$. We typically used 400 mesh point per layer and the time step $d_\tau = 0.3 d_u/\ell \approx 2\times 10^{-4}$. The total simulation time is typically 200 in reduced units for every current point.

[1] R. Kleiner, F. Steinmeyer, G. Kunkel, and P. Müller, Phys. Rev. Lett. **68**, 2394 (1992); R. Kleiner and P. Müller, Phys. Rev. B **49**, 1327 (1994).

[2] L. N. Bulaevskii and A. E. Koshelev, Phys. Rev. Lett. **99**, 057002 (2007).

[3] L. Ozyuzer, A. E. Koshelev, C. Kurter, N. Gopalsami, Q. Li, M. Tachiki, K. Kadowaki, T. Yamamoto, H. Minami, H. Yamaguchi, T. Tachiki, K. E. Gray, W.-K. Kwok, and U. Welp, Science **318**, 1291 (2007); K. Kadowaki, H. Yamaguchi, K. Kawamata, T. Yamamoto, H. Minami, I. Kakeya, U. Welp, L. Ozyuzer, A. Koshelev, C. Kurter, K. E. Gray, and W.-K. Kwok, Physica C **468**, 634 (2008).

[4] A. E. Koshelev and L. N. Bulaevskii, Phys. Rev. B **77**, 014530 (2008).

[5] Sh. Lin and X. Hu, Phys. Rev. Lett. **100**, 247006 (2008).

[6] S. Sakai, P. Bodin, and N. F. Pedersen, J. Appl. Phys. **73**, 2411 (1993); L. N. Bulaevskii, D. Domínguez, M. P. Maley, A. R. Bishop, and B. I. Ivlev, Phys. Rev. B **53**, 14601 (1996); S. N. Artemenko and S. V. Remizov, JETP Lett. **66**, 853 (1997).

[7] M. Machida, T. Koyama, and M. Tachiki, Phys. Rev. Lett. **83**, 4618 (1999); R. Kleiner, T. Gaber, and G. Hechtfischer, Phys. Rev. B **62**, 4086 (2000); S. Madsen and N. F. Pedersen, *ibid.* **72**, 134523 (2005); M. Tachiki, M. Iizuka, K. Minami, S. Tejima, and H. Nakamura, *ibid.* **71**, 134515 (2005); B. Y. Zhu, H. B. Wang, S. M. Kim, S. Urayama, T. Hatano, and X. Hu, *ibid.* **72**, 174514 (2005); S. Savelev, V. Yampolskii, A. Rakhmanov, and F. Nori, *ibid.* **72**, 144515 (2005); S. Lin, Xiao Hu, and M. Tachiki, *ibid.* **77**, 014507 (2008).

[8] See EPAPS Document No. E-PRBMDO-78-118837 for animations of dynamic configurations of the phases and electric fields. For more information on EPAPS, see http://www.aip.org/pubservs/epaps.html.

[9] This alternating solution with the periodicity 1-2-1-2-… is not the only possible state. The solution with the periodicity 1-1-2-2-1-1-… also can be built in a similar way.

[10] T. A. Fulton and R. C. Dynes, Solid State Commun. **12**, 57 (1973); P. S. Lomdahl, O. H. Soerensen, and P. L. Christiansen, Phys. Rev. B **25**, 5737 (1982).

[11] G. Costabile, S. Pagano, and R. D. Parmentier, Phys. Rev. B **36**, 5225 (1987).

[12] J. T. Chen, T. F. Finnegan, and D. N. Langenberg, Proceedings of the International Conference on Superconductivity, Stanford, 1969, edited by F. Chilton (North-Holland, Amsterdam, 1971) [Physica (Amsterdam), **55**, 413 (1971)].